ADVANCED FUNCTIONAL MATERIALS
www.afm-journal.de

Kinetic Isotope Effect in the Hydrogenation and Deuteration of Graphene

Alessio Paris, Nikolay Verbitskiy, Alexei Nefedov, Ying Wang, Alexander Fedorov, Danny Haberer, Martin Oehzelt, Luca Petaccia, Dmitry Usachov, Denis Vyalikh, Hermann Sachdev, Christoph Wöll, Martin Knupfer, Bernd Büchner, Lucia Calliari, Lada Yashina, Stephan Irle,* Alexander Grüneis**

Time-dependent photoemission spectroscopy is employed to study the kinetics of the hydro-genation/deuteration reaction of graphene. Resulting in an unusual kinetic isotope effect, the graphene deuteration reaction proceeds faster than hydrogenation and leads to substantially higher maximum coverages of deuterium (D/C≈35% vs H/C≈25%). These results can be explained by the fact that in the atomic state H and D have a lower energy barrier to overcome in order to react with graphene, while in the molecular form the bond between two atoms must be broken before the capture on the graphene layer. More importantly, D has a higher desorption barrier than H due to quantum mechanical zero-point energy effects related to the C–D or C–H stretch vibration. Molecular dynamics simulations based on a quantum mechanical electronic potential can reproduce the experimental trends and reveal the contribution of the constituent chemisorption, reflection, and associative desorption processes of H or D atoms onto graphene. Regarding the electronic structure changes, a tunable electron energy gap can be induced by both deuteration and hydrogenation.

1. Introduction

Kinetic isotope effects (KIEs), i.e., a different reaction constant for isotopes, are important phenomena in physical chemistry. They have been studied for a long time in their relation to the activation and rate of chemical reactions.[1] A significant contribution to KIE are vibrational zero-point energy (ZPE) effects that upshift the energy of a chemical bond by half the phonon frequency of its constituents (given the temperature at which our experiment is performed, only the ground state of the harmonic oscillator is relevant). Hence, KIEs are easy to observe in the hydrogen isotopes (deuterium and tritium) due to their large relative mass difference and were studied, even at the single-molecule level,[2] for hydrogen

Dr. A. Paris, Dr. L. Calliari
Interdisciplinary Laboratory for Computational Science (LISC)
FBK-CMM, via Sommarive 18, I-38123 Trento, Italy
N. I. Verbitskiy
Department of Materials Science
Moscow State University
Leninskiye Gory, 1/3, 119992 Moscow, Russia
Faculty of Physics, University of Vienna
Boltzmanngasse 5, A-1090 Vienna, Austria
Dr. A. Nefedov, Prof. C. Wöll
Institut für Funktionelle Grenzflächen (IFG)
Karlsruher Institut für Technologie (KIT)
Hermann-von-Helmholtz- Platz 1
D-76344 Eggenstein-Leopoldshafen, Germany
Dr. Y. Wang, Dr. S. Irle
Department of Chemistry
Graduate School of Science
Nagoya University
Nagoya 464-8602, Japan
E-mail: ywang@iar.nagoya-u.ac.jp; sirle@chem.nagoya-u.ac.jp
A. V. Fedorov
IFW Dresden, P.O. Box 270116, D-01171 Dresden, Germany
St. Petersburg State University St. Petersburg
198504, Russia
Dr. D. Haberer, Dr. M. Knupfer, Dr. B. Büchner
IFW Dresden, P.O. Box 270116, D-01171 Dresden, Germany
Dr. M. Oehzelt
Helmholtz-Zentrum Berlin für Materialien und Energie
Elektronenspeicherring BESSY II
Albert-Einstein-Strasse 15, D-12489 Berlin, Germany
Dr. L. Petaccia
Elettra Sincrotrone Trieste
Strada Statale 14 Km 163.5, 34149 Trieste, Italy
Dr. D. Usachov
St. Petersburg State University St. Petersburg
198504, Russia
Dr. D. V. Vyalikh
St. Petersburg State University St. Petersburg
198504, Russia
Institut für Festkörperphysik TU Dresden
Mommsenstrasse 13, D-01069 Dresden, Germany
Dr. H. Sachdev
Max-Planck-Institut für Polymerforschung
Ackermannweg 10, D-55128 Mainz, Germany
Dr. L. V. Yashina
Department of Chemistry
Moscow State University
Leninskiye Gory, 1/3, 119992 Moscow, Russia
Dr. A. Grüneis
IFW Dresden, P.O. Box 270116, D-01171 Dresden, Germany
Faculty of Physics, University of Vienna
Boltzmanngasse 5, A-1090 Vienna, Austria
E-mail: alexander.grueneis@univie.ac.at

DOI: 10.1002/adfm.201202355

transfer in organic reactions including acid and base catalysis, enzyme reactions and catalytic decomposition.[3] Most of these reactions were carried out with H and D in a molecular configuration and it was found that the reaction constant for the D compounds is lower than for the corresponding H compounds. These results are explained by the larger ZPE for H bonds, which results in a lower potential energy barrier to be overcome for H-bonds breaking as compared to D bonds. As a result, the bond-breaking reaction proceeds faster for the H compound than for the D compound. Similarly, recent simulations have shown that laser irradiation of hydrogenated/deuterated graphene causes H to desorb from the central carbon atom of pyrene, whereas D remains adsorbed on the surface.[4] There have been very few reports on experiments carried out with one reactant being atomic H or D such as the H-D exchange reactions[5,6] or reactions of H(D) with oxygen[7] where it was found that the oxygen-H(D) reaction proceeds equally fast for D and H. This was attributed to the absence of vibrational zero-point energy effects for the atomic species. Much less is known about the kinetics of these reactions in functional carbon materials based on hydrogenated graphene,[8] such as novel 2D polymers.[9]

Herein, we present a novel inverse kinetic isotope effect involving the reaction of H/D radicals with the carbon atoms of epitaxial graphene. Graphene serves as an ideal two-dimensional model for covalent functionalization[10] with hydrogen,[8,11–15] fluorine,[16,17] nitrogen,[18,19] oxygen[20,21] as well as with small organic molecules.[22] Effects due to the interchange of ^{12}C and ^{13}C isotopes have been investigated particularly in the engineering of carbon materials with controlled isotope constituents.[23] The advantages of graphene include a flat, well ordered large area surface with constant density of atoms. Therefore, the time-dependence of stoichiometry, which is necessary to describe the kinetics, can be precisely controlled and measured. Previously, we have shown that high resolution C 1s core-level X-ray photoemission spectroscopy (XPS) directly yields the stoichiometry of hydrogenated graphene (H-graphene) due to the chemical shift between hydrogenated and un- hydrogenated carbon atom peaks, and it allows time-dependent graphene hydrogenation to be studied in situ.[9] In a similar manner, we here determine the C–H and C–D stoichiometries by XPS for a time-dependent series of hydrogenation and deuteration reactions for a monolayer of graphene from the pristine state up to the maximum H or D coverage. In addition, we used the near-edge X-ray absorption fine structure (NEXAFS), which is sensitive to the number of H or D atoms chemisorbed on graphene as it reduces the π^* resonance intensity in the absorption spectrum, to independently confirm the different saturation of the two atomic species. Further, we model the measured time-dependent C/H and C/D stoichiometries by a first order adsorption model which yields the values of reflection, chemisorption and associative desorption probabilities[9] of H and D atoms. In addition, we perform quantum-mechanical molecular dynamic (QM/MD) simulations of the hydrogenation/deuteration process and model calculations for the potential energy curves of the adsorption process of H/D on a coronene molecule. To directly investigate the changes of the electronic band structure and investigate a possible electronic isotope effect, we perform angle-resolved photoemission spectroscopy (ARPES) as a function of deuterium chemisorbed by graphene.[15] We will show that a pronounced isotope effect is observable in the chemisorbtion of D and H on a graphene monolayer, resulting in a faster rate of absorption and a higher saturation coverage for the former than for the latter. Moreover, the experimental results are interpreted through a phenomenological model applied to the collected data and are also correctly reproduced by the quantum-mechanical simulation.

2. Results and Discussion

2.1. The Reaction Product: Fully H/D Saturated Graphene

Quasi-free-standing graphene on Au/Ni/W was synthesized in-situ by chemical vapor deposition (CVD)[15,24,25] and exposed for a definite period of time to a beam of atomic hydrogen[9,15] or deuterium. This leads to formation of C–H and C–D bonds perpendicular to the graphene plane.[8] The associated vibrational energy of the C–H (C–D) vibration along the bond axes is estimated to be very similar to that of H(D) on graphite giving 2650 cm^{-1} (1950 cm^{-1}),[26,27] which amount to a difference of 700 cm^{-1} or equivalently 87 meV. The large energy difference between C–H and C–D vibration is important for ZPE effects. After each hydrogenation/deuteration step we recorded the C 1s photoemission spectra to determine the H/C and D/C ratios. Upon hydrogenation or deuteration the C 1s line is represented by the convolution of three different contributions:[15] pristine graphene carbon atoms (hereafter called C1 component), carbon atoms with a deuterated/hydrogenated neighbor (C2) and atoms that have C–D or C–H bonds (C3). The three components were fitted with Doniach–Sunjic lineshapes. We can estimate the H/C or D/C ratio η according to $\eta = C3/(C1 + C2 + C3)$. The C 1s spectra for H/D saturated graphene layer are shown in **Figure 1**a. We show here only the C3 components as they demonstrate the difference between the D/C ratio and the H/C ratio. The high binding energy shoulder (C3 component) of the C 1s line corresponds to a chemical shift due to formation of C–H/C–D bonds and thus the H/C and D/C stoichiometries can be conveniently obtained with an accuracy of ≈1%. As it is clearly seen from Figure 1a, the H-graphene saturation (H/C≈25%) and D-graphene saturation (D/C≈35%) differ significantly. This fact is corroborated by NEXAFS spectra displayed in Figure 1b (additional spectra for different incidence angles of light are included in the supplementary information). We observe that the intensity of the π^* resonance peak is remarkably lower for completely deuterated graphene than for fully hydrogenated graphene, confirming the higher saturation of carbon 2pz orbitals perpendicular to graphene and, hence, the corresponding decrease of the number of in-plane π bonds.

2.2. Reaction Kinetics

The higher D/C ratio vs. H/C ratio was observed at all exposure times. In **Figure 2**a two series of C 1s spectra at selected exposure times for graphene hydrogenation and deuteration are presented (the full dataset is shown in the supplementary information). One can conclude that deuterium chemisorption

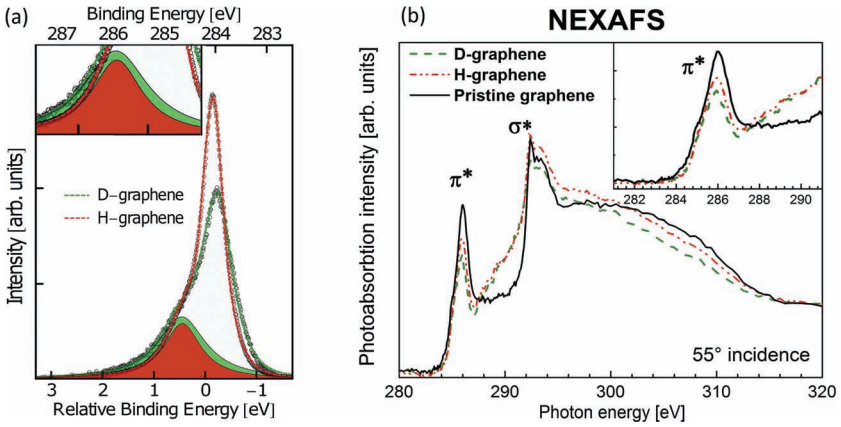

Figure 1. (a) C 1s core-level spectra of fully hydrogenated graphene (H-graphene) and fully deuterated graphene (D-graphene). The H/C and D/C ratios are 25% and 35%, respectively. The red (green) line represents the fit to experimental data for H-graphene (D-graphene), while the red area (red+green area) is the C3 contribution from carbon atoms bonded to hydrogen (deuterium). Experimental spectra are normalized to the area under each curve. The inset depicts a magnification of the C3 component. (b) Carbon K-edge NEXAFS spectra taken at 55° between the polarization vector and the surface normal, for pristine graphene, fully hydrogenated and fully deuterated graphene. Spectra are normalized to a common intensity for photon energies between 320 and 330 eV.

proceeds faster and reaches a higher final coverage as compared to hydrogen chemisorption, thus the KIE is confirmed over the whole chemisorption series. As we will discuss later, this is a direct consequence of the ZPE effects which are responsible for faster formation of stronger C–D bonds as compared to C–H bonds. Moreover, comparing the ≈25% coverage data for deuterated graphene (t = 6000 s) and hydrogenated graphene (t = 20 000 s), we note that the deuterated graphene has a considerably larger C1 component in the fit. This is a direct consequence of the lower aromaticity of the deuterated compound with respect to the hydrogenated compound. An ideal C_4H compound would have a zero C1 component but this is not the case for C_4D as we will discuss later in the context of possible chemisorption patterns.

Next, we investigate the H-D exchange reaction by exposing a fully hydrogenated (deuterated) graphene to D(H) atoms. Since the chemical shift in C 1s spectra for D- and H-bonded carbon atoms is indistinguishable within XPS experimental resolution, it is hardly possible to prove the existence of a mixed H/D chemisorbed phase. We are able however, to study whether fully hydrogenated graphene (25%) is still susceptible to further deuteration or whether it is completely inert. Similarly, we study the opposite problem whether we can reverse the 35% D/C ratio to a 25% H/C ratio by exposing a fully deuterated graphene to a beam of H (this would happen if all D atoms were to be replaced by H atoms via H-D associative desorption). In Figure 2b we show that D chemisorption on fully hydrogenated graphene increases the coverage up to 29.5%, which suggests that D reacts with graphene C atoms in between C–H bonds. It also means that only partial H-D exchange may occur, because full H-D exchange would result in a coverage of 35%. On the other hand, exposing the fully deuterated graphene to hydrogen does not reduce the coverage as one might expect for D-H exchange and does not reduce the recovery of the C_4H structure typical of hydrogenated graphene.[9] Hence we suggest that the more stable deuterium bond causes D to be is harder to remove from the surface than H by associative desorption.

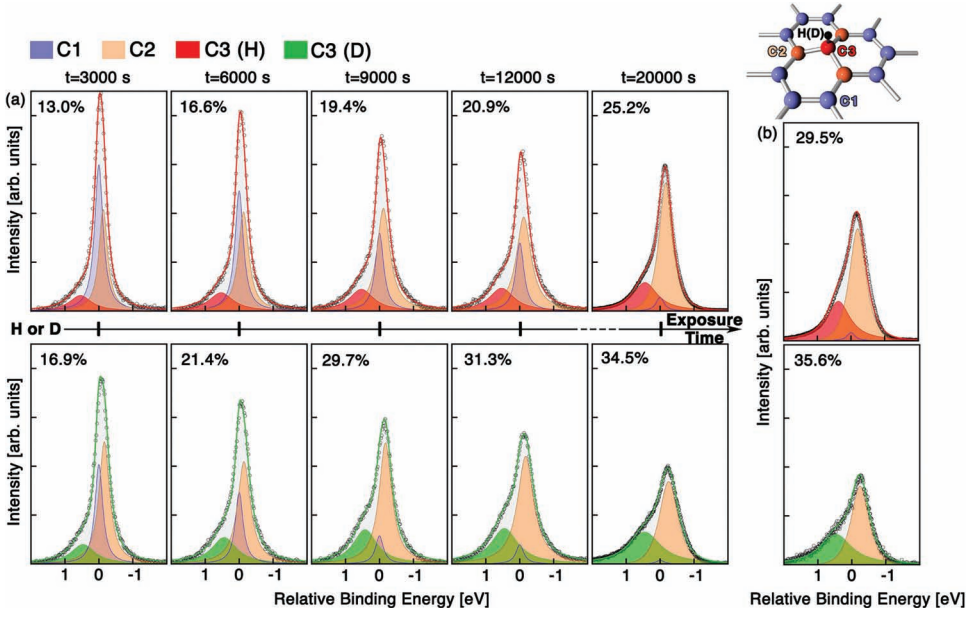

Figure 2. a) Time series of C 1s core-level spectra of graphene as a function of exposure to hydrogen (upper row) and to deuterium (lower row). The number denotes the atomic percentage of H/C and D/C atoms. All C 1s features are fitted with Doniach–Sunjic line shapes with components C1 (blue) and C2 (orange) representing unhydrogenated C atoms of graphene, while C3 (red or green) is the contribution from carbon bonded to hydrogen or deuterium. C1 has no neighboring C–H (C–D) bond and C2 has a neighboring C–H(C–D) bond. b) XPS spectra for fully hydrogenated graphene exposed to deuterium (upper plot) and fully deuterated graphene exposed to hydrogen (lower plot).

The coverage datasets for hydrogenation and deuteration are shown in **Figure 3**a along with a fit derived from a model describing first order chemisorption (see the Experimental Section). The higher saturation and the faster reaction rate for D-graphene is also evident from this graph. The fit to the chemisorption model allowed us to extract the values of adsorption, reflection and associative

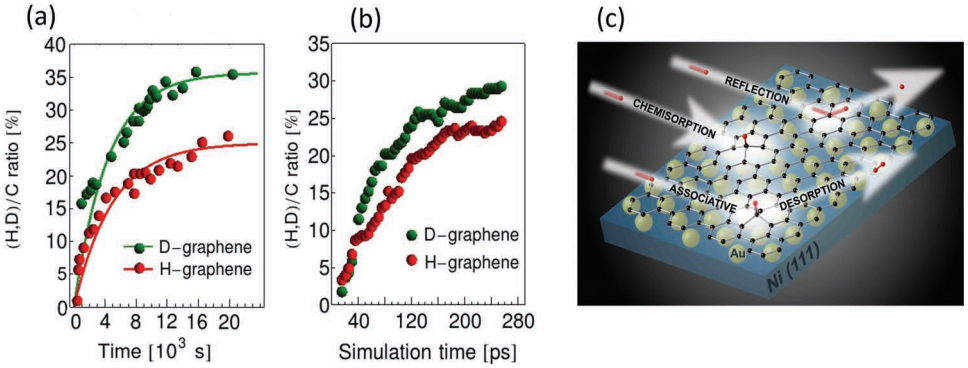

Figure 3. a) H/C and D/C ratios determined by XPS (points) along with the best fit for the chemisorption curve from 2. b) H/C and D/C ratios determined by simulation. c) Sketch of the H/D reflection, chemisorption, and associative desorption processes on the graphene surface that were found to be relevant in the QM/MD simulations and included in the phenomenological model.

desorption probabilities [P_{ads}, P_{refl} and PX2 (X = H or D)]. A sketch of the relevant processes is shown in Figure 3c.

Two sets of the fitting parameters describing the experimental results for hydrogenation and deuteration are listed in **Table 1**. These values are in line with the observation that deuterium chemisorption proceeds faster and hydrogen abstraction from graphene by associative desorption is easier than for deuterium. Since the sum of all probabilities must equal one, the probability of reflection is higher for H than for D. We stress that this simple phenomenological model relies on the assumption of coverage-independent probabilities and neglects the possibility of higher order corrections to the curves of Figure 3a.

In order to get a deeper insight into the chemisorption process, we also performed QM/MD simulations of the graphene hydrogenation/deuteration kinetics. Simulations of similar systems have been done before, using a different approach.[28,29] These simulations do not depend on parameters extracted from our experimental results (see the Experimental Section for details). The results are shown in Figure 3b. The difference in the time scale between experimental and simulation data is due to a different H/D atom flux (the values are reported in the Experimental Section). The atom flux of the simulation was chosen to be compatible with the time scale of typical QM/MD simulation and this justifies the much shorter time scale on which the simulated chemisorption takes place. Taking into account this time rescaling, the overall trend of higher D/C ratios and higher D/C saturation is well reproduced on a qualitative level. The differences between experimental and simulated data can be explained in terms of (1) quantum tunneling effects of H which would enhance the spread between the H and D curves and (2) the fact that in the simulations a monochromatic H/D beam with a projectile kinetic energy of 0.4 eV has been used while the actual atomic velocities are described by a Maxwell–Boltzmann distribution.

Table 1. Probabilities of chemisorption (P_{ads}), reflection (P_{refl}) and associative desorption P_{H2} (P_{D2}) for an incoming H or D atom, as derived by the fit to the experimental data in Figure 3a.

Probability	P_{ads}	P_{H2} (P_{D2})	P_{refl}
hydrogenation	0.036	0.108	0.856
deuteration	0.058	0.104	0.838

2.3. Reaction Path

As a complement to the QM/MD simulations we also performed static calculations of the energy levels of the reactant, transition state and product of the H/D chemisorption and associative desorption processes on the central C atoms of coronene, a model molecule for graphene. Even though coronene is a relatively small molecule with a large HOMO-LUMO gap, reaction energies for graphene hydrogenation and hydrogenation of coronene on its central hexagon are remarkably similar.[30] The reason for choosing the coronene molecule as a model system in this case was that barrier heights can be calculated with much greater accuracy than for extended graphene.

For the sake of simplicity, in the following discussion we assume collinear spin orientation but note that in general, non-collinear spin orientations are possible. The calculated potential energy curves of H and D on coronene are depicted in **Figure 4**a,b. In these Figures and in the following discussion the reactant (R), transition state (TS) and product (P) are labeled with numbers for the spin multiplicity and "a" or "d" for chemisorption or associative desorption, respectively. Chemisorption proceeds from the ground state (^2R_a) or an excited state of coronene (^4R_a) following a previous chemisorption and associative desorption of two H (D) atoms with the same spin. After chemisorption in a ^2R_a state, the H(D) atom has to overcome a potential energy barrier of 0.29 eV to the transition state ^2TS_a. Along this path, a weak C–H or C–D bond is formed and the ZPE effects enhance the chance of reflection of H into the vacuum as it travels along this path. Once it is chemisorbed (^2P_a), deuterium has a considerably stronger bond to carbon than H due to ZPE effects. In this state, the red (green) lines denote the energy of the C–H (C–D) bond. Their energy difference is equal to the difference between the C–H and C–D vibrational energies. They amount to 2738 and 2005 cm^{-1} for the C–H and C–D vibration, respectively. These facts alone can already explain the observations of faster chemisorption of D and a higher reflectivity for H atoms. However, this explanation does not provide the entire picture. We must further consider the process of associative

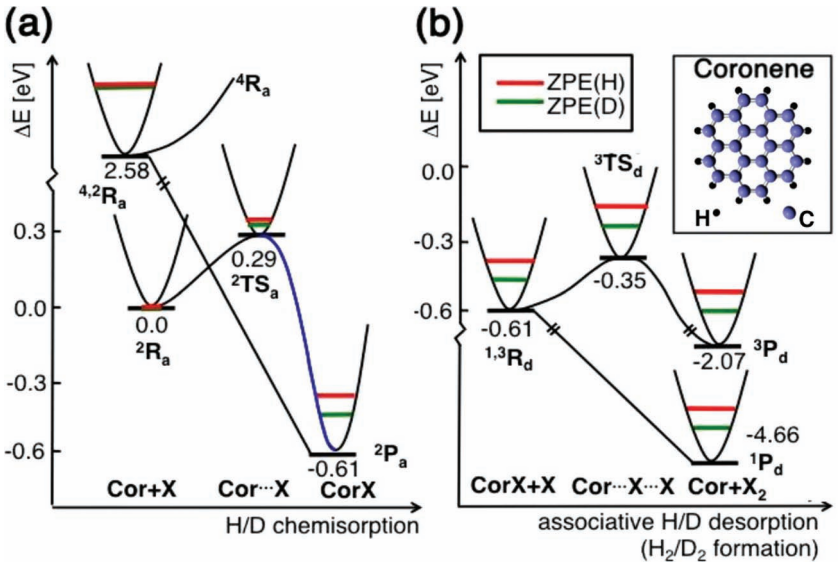

Figure 4. a) Potential energy curves and barriers for the different stages of hydrogen (red lines) and deuterium (green lines) chemisorption on coronene. Note the differences of C–H and C–D bonds due to ZPE effects after chemisorption. Cor+X is the initial state with a free H or D atom, Cor· · ·X is the transition state, while CorX is the final stage with an adsorbed H or D on coronene. b) Energy potential curves of H and D for the stages of an associative desorption process (the inset shows a sketch of the coronene molecule). CorX+X is the initial state with one free and one adsorbed H or D atom, Cor· · ·X· · ·X is the transition state, while Cor+X2 is the final stage with the molecule leaving coronene. The meaning of the labels appearing in both figures is fully explained in the text.

desorption presented in Figure 4b. In this process the electron spin of the incoming H(D) atom can be parallel or antiparallel to the spin of the coronene-H(D) complex.

Since coronene is a closed-shell molecule, its state after chemisorption and the subsequent associative desorption is governed by the spins of the electrons of the two H(D) atoms. If the spins are parallel, coronene is left in an excited triplet state (^3P_d) and if these spins are antiparallel, coronene is left in its singlet ground state (^1P_d). Notably, there exists a barrier for chemisorption of a second atom with the same spin (^3TS_d). If left in its excited triplet state, coronene after H/D abstraction is significantly more reactive and does not pose a reaction barrier for the chemisorption of another atom (see Figure 4a-state ^4R_a). The fact that we can produce triplet states (^3P_d) by repeated H/D chemisorption is extremely interesting by itself, since such states are usually generated by electronic excitation. In the present case, graphene with a metallic substrate, these states can undergo radiationless decay to the singlet ground state, while in free-standing graphene they might indeed play a role in chemical transformations.

Despite its importance to understand the energy barriers involved, the potential energy curves are not sufficient to describe all aspects of the kinetics of hydrogenation/deuteration in a comprehensive way. We therefore discuss some additional features beyond the static potential energy diagrams and related to the dynamics and geometry of the system. First, assuming we have the same energy of the incoming H/D atom, the velocity of deuterium atoms will be smaller and, therefore, the increased reaction time leads to higher chemisorption probabilities. This fact is evident from both the phenomenological model and the QM/MD simulations. Second, the reaction rate for associative desorption is also influenced by the geometry of the adsorbed radical: we have found that the larger C–H bond length enhances the associative desorption of H in comparison to D.

Given the saturation point D/C≈35%, questions regarding the preferred chemisorption pattern and aromaticity of D-graphene emerge, as it has been already discussed for H-graphene.[9] From a comparison of the QM/MD simulation of the two we find that the number of aromatic rings per unit area is higher for H-graphene than for D-graphene (see **Figure 5**). The tendency towards higher aromaticity in hydrogenated graphene as compared to deuterated graphene also manifests itself in the ratio of the probabilities P_{ads} and P_{X2} which governs the final coverage as can easily be seen when considering Equation (2) for very large values of the exposure time. Consequently, the C_4H stoichiometry allows in theory for a 100% aromatic compound[9] while the two proposed structures for deuterated graphene with stoichiometries $C_{3.2}D$ and $C_{2.7}D$ (see Figure 5) are less aromatic. This could be related to the higher diffusion rate for hydrogen on graphene as compared to deuterium, which is also a consequence of stronger C–D bonds than C–H bonds.[31] Thus, we conclude the ZPE effects directly influence the aromaticity of hydrogenated/deuterated graphene compounds via the stoichiometry.

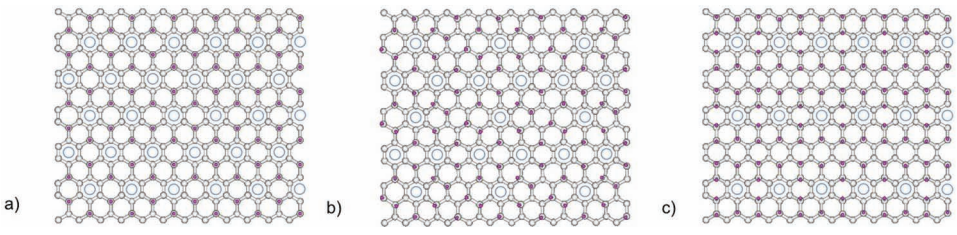

Figure 5. a) Final configuration of hydrogenated graphene. A C_4H structure with aromatic rings is achieved. b,c) Possible final configuration for deuterated graphene. The two geometries correspond to final structures $C_{3.2}D$ and $C_{2.7}D$, respectively.

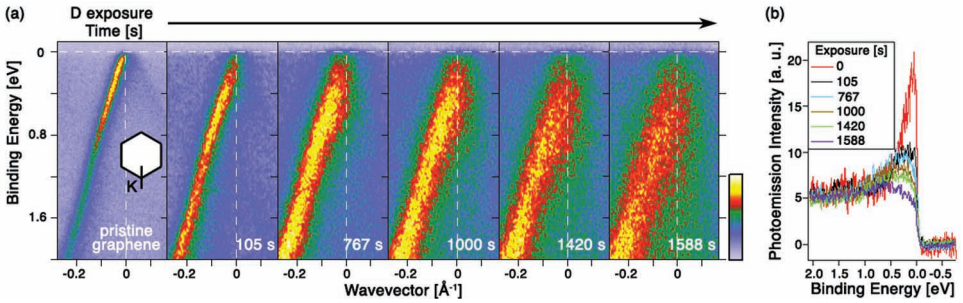

Figure 6. a) ARPES spectra close to the K point for increasing D chemisorption. The direction of measurement is indicated in the 2D Brillouin zone and the time of exposure is denoted in each spectrum. b) Electron energy dispersion curves at the K point for this chemisorption series. A common intensity scale for all D doping levels is used.

2.4. Electronic Isotope Effect

Finally, we discuss the impact of deuteration on the electronic band structure of graphene. Through an analysis of the spectral function we are able to determine possible differences between the electronic structure of chemisorbed deuterium and hydrogen and the relevance of an electronic isotope effect. To this end, we performed angle-resolved photoemission spectroscopy (ARPES) studies in the proximity of the K point of graphene where the π band touches the Fermi level.[15,32,33] The series of ARPES measurements with increasing D exposure are shown in **Figure 6**a. It can be seen that upon deuteration, the band broadens and the photoemission intensity at the Fermi level gets weaker, while a band gap opens between the band and the Fermi energy. This is similar to the trends observed for hydrogen[15] on graphene and is confirmed by the individual energy dispersion curves through a K point shown in Figure 6b. Hence, we conclude that deuterium- doped graphene develops a band-gap similar to that observed for hydrogen,[15] and consequently that the electronic isotope effect is weak.

3. Conclusions

To sum up, we have observed a strong inverse kinetic isotope effect (KIE) for the hydrogenation/deuteration reaction on quasi-free-standing monolayer graphene leading to substantially higher saturation coverage of D as compared to H. This is an extremely unusual KIE and could be explained by the fact that one reactant is a H/D atom. For molecules, the vibrational zero-point energy (ZPE) effects which make the breakup of D_2 more difficult than H_2 would reduce the rate at which atomic D is supplied and hence cause the usually observed behavior with the deuterium reaction proceeding slower. Moreover, the ZPE effect promotes the chemisorption of D in the sense that it makes reflection less likely, because as soon as a partial C–D bond is formed, the ZPE effect makes the C–D bond more stable than the C–H bond. The unique geometry of the experiment and the relatively low flux of H/D atoms allowed us to study the surface chemistry of graphene during hydrogenation/deuteration monitoring the whole reaction in situ and in real time by photoemission spectroscopy. The experimental results for hydrogenation/deuteration are well described using a phenomenological kinetic model with terms for chemisorption, associative desorption and reflection of H/D atoms. Probabilities for these processes were fitted to the experimental stoichiometries as a function of H/D exposure. They could qualitatively be explained using potential energy curves, C–H/C–D bond lengths and considering the interaction times of D or H with the graphene surface. All this also enters the QM/MD simulations which manage to reproduce the experimental results. The observed significant difference in the reaction involving H and D with graphene is relevant for isotope specific chemical reactivity in functional carbon materials and is important for the intensive research regarding atomic control of chemical reactivity at the nanoscale.

4. Experimental Section

Monolayer graphene was prepared under ultrahigh vacuum conditions by chemical vapor deposition on Ni(111) thin films epitaxially grown on W(110).[25] A monolayer of Au was then deposited and intercalated into the interface between Ni and graphene, making the latter quasi-free-standing.[15] The graphene layer was then exposed to hydrogen[9,15] or deuterium atomic gas beams, obtained by thermal cracking in a tungsten capillary at $T = 3000$ K. The maximum surface coverage was obtained after several hydrogenation or deuteration steps for different periods of time. The pressure in the analysis chamber was kept at 1×10^{-6} mbar during the hydrogenation/deuteration steps. In the case of deuteration, a 2% pressure increase was applied to take into account the smaller sensitivity of the pressure gauge to deuterium as compared to hydrogen.[34]

Experimental data were acquired at the following facilities: XPS and NEXAFS measurements were performed at HESGM and UE-52 beamlines at synchrotron BESSY II (Germany). ARPES measurements were done at the BaDElPh beamline at Elettra synchrotron (Italy).[35] The time-dependent chemisorption series were carried out with graphene at room temperature. For all XPS measurements we used a photon energy of $h\omega = 400$ eV and a total energy resolution of 30 meV. ARPES measurements in the vicinity of the K point of graphene were carried out at a photon energy $h\omega = 26$ eV with the sample at 26 K yielding a total energy resolution of 15 meV.

H/D atom chemisorption on graphene was simulated by a non-equilibrium QM-MD simulation based on a self-consistent-charge density-functional tight-binding quantum chemical potential. On the basis of the Born-Oppenheimer (BO) approximation, we computed total electronic energy and forces on the nuclei on the fly at each time step of the trajectories, and performed the time propagation of the position of the nuclei using Newtons classical equation of motion. Our graphene model system consisted of 32 carbon atoms with a planar

unit cell (9.856 Å × 8.596 Å × 100 Å) with periodic boundary conditions (PBC). In ten trajectory replica for each isotope, H or D atoms were placed in randomly chosen positions at a distance of 4 Å, with initial velocities corresponding to 0.4 eV kinetic energy aimed perpendicularly to the target graphene surface. The spin on each H or D atom was randomly selected, and total spin of the system during the QM/MD simulations was defined at any time as the cumulative sum of all spins of the projectiles. The rate was one H/D projectile every 0.5 ps and the resulting flux was $I \approx 0.0625$ atoms per picosecond per carbon atom. Ten trajectory replicas were generated, up to 250 ps simulated time (500 atoms). The incident kinetic energy of 0.4 eV is just barely enough to overcome the chemisorption barrier for H/D on the BO potential energy surface and our modified spin-polarized, self-consistent-charge density-functional tight-binding (SDFTB) potential correctly reproduces this barrier.[36] In order to analyze the results of the QM/MD simulations, we performed a traditional quantum chemical study of chemical reaction pathways based on the characterization of stationary points on the Born–Oppenheimer (BO) potential energy surfaces (PESs) using harmonic frequency analysis. The latter allows for the estimation of the vibrational zero-point energy contribution to the first-order kinetic isotope effects, as well as for the contribution of tunneling following the Wigner correction. For this purposes, we employed both first principles density functional theory (DFT) as well as SDFTB approaches. The DFT calculations were carried out using the B3LYP functional in combination with the cc-pVDZ basis sets as implemented in the GAUSSIAN 03 suite of programs. We accepted the default convergence criteria, and performed harmonic vibrational frequency analysis based on analytical second energy derivatives with respect to the nuclear positions. DFT calculations were carried out using the spin-unrestricted approach using collinear spin functions as necessary. Based on these B3LYP/cc-pVDZ optimized geometries, we performed additional single-point energy calculations using the SDFTB method. The latter was carried out using the standard mio-0-1 parameter set except for the C–H repulsive potential, which was modified to mimic a ROCCSD(T)/cc-pVTZ-quality PES of coronene hydrogenation.

Regarding the phenomenological model, the experimental curves of C/H and D/H stoichiometry ratio η versus exposure time t were modeled by the following differential equation,[9]

$$\frac{d\eta}{dt} = I P_{\text{ads}}(1-\eta) - I P_{X2}\eta \quad (1)$$

where I is the atom flux, estimated as $I \approx 0.0014$ atoms per second per carbon atom. For deuterium, the flux was estimated to be 3% higher than hydrogen, due to the different pumping speed of the turbomolecular pump reported in its manual. The differential equation contains terms for H(D) atom chemisorption and associative desorption. The obtained datasets allow us to to perform a quantitative comparison of the relevant probabilities for chemisorption (P_{ads}), reflection (P_{refl}) and associative desorption (P_{X2}) for both H and D on graphene. The probabilities are interrelated to each other by the relation $P_{ads} + P_{X2} + P_{refl} = 1$. The solution to the differential equation is given by[9]

$$\eta\,[\%] = 100 \times \frac{P_{\text{ads}}}{P_{\text{ads}} + P_{X2}} \left(1 - e^{-I(P_{\text{ads}}+P_{X2})t}\right) \quad (2)$$

Supporting Information

Supporting Information is available from the Wiley Online Library or from the author.

Acknowledgements

A.P. recognizes that his work is partially funded by Fondazione Caritro under the project Mistico. N.V. acknowledges partial funding under RFBR grant No. 12-03-01149. Y.W. and S.I. thank Mr. Yoshifumi Nishimura for assistance with the calculation of DFTB ZPEs. The theoretical work was supported by a NINS Program for Cross-Disciplinary Study. D.H., A.V.F., M.K. and A.G. acknowledge a DFG project GR 3708/1-1. D.H. and A.G. acknowledge funding from the European Community's Seventh Framework Program (FP7/2007-2013) under grant agreement 226716 for their stay at the Elettra synchrotron. D.H., L.P., and A.G. thank D. Lonza for his technical assistance during the experiments at Elettra. D.U. acknowledges funding from RFBR, SPbSU and President's grant MK-3303.2012.2. A.P. and A.G. thank the Helmholtz Centre of Berlin for financial support during their stay at BESSY II synchrotron. A.G. acknowledges an APART fellowship from the Austrian Academy of Sciences. This work was partially supported by NanoMikro Programme (KIT, Karlsruhe).

Received: August 17, 2012
Revised: October 8, 2012
Published online: November 2, 2012

[1] F. Westheimer, *Chem. Rev.* **1961**, *61*, 265.
[2] S. Lu, W. Li, D. Rotem, E. Mikhailova, H. Bayley, *Nat. Chem.* **2010**, *2*, 921.
[3] K. B. Wiberg, *Chem. Rev.* **1955**, *55*, 713.
[4] J. Harujama, K. Watanabe, *Surf. Sci Nanotechnol.* **2011**, *9*, 1.
[5] A. Farkas, L. Farkas, *Proc. R. Soc. London, Ser. A* **1935**, *152*, 124.
[6] H. Steiner, E. K. Rideal, *Proc. R. Soc. London, Ser. A* **1939**, 173, 503.
[7] M. G. Evans, *J. Chem. Phys.* **1934**, *2*, 726.
[8] D. C. Elias, R. R. Nair, T. M. G. Mohiuddin, S. V. Morozov, P. Blake, M. P. Halsall, A. C. Ferrari, D. W. Boukhvalov, M. I. Katsnelson, A. K. Geim, K. S. Novoselov, *Science* **2009**, *323*, 610.
[9] D. Haberer, C. E. Giusca, Y. Wang, H. Sachdev, A. V. Fedorov, M. Farjam, S. A. Jafari, D. V. Vyalikh, D. Usachov, X. Liu, U. Treske, M. Grobosch, O. Vilkov, V. K. Adamchuk, S. Irle, S. R. P. Silva, M. Knupfer, B. Büchner, A. Grüneis, *Adv. Mater.* **2011**, *23*, 4497.
[10] J. M. Englert, C. Dotzer, G. Yang, M. Schmid, C. Papp, J. M. Gottfried, H.-P. Steinrueck, E. Spiecker, F. Hauke, A. Hirsch, *Nat. Chem.* **2011**, *3*, 279.
[11] S. Ryu, M. Y. Han, J. Maultzsch, T. F. Heinz, P. Kim, M. L. Steigerwald, L. E. Brus, *Nano Lett.* **2008**, *8*, 4597.
[12] P. Sessi, J. R. Guest, M. Bode, N. P. Guisinger, *Nano Lett.* **2009**, *9*, 4343.
[13] A. Bostwick, J. L. McChesney, K. V. Emtsev, T. Seyller, K. Horn, S. D. Kevan, E. Rotenberg, *Phys. Rev. Lett.* **2009**, *103*, 056404.
[14] R. Balog, B. Jorgensen, L. Nilsson, M. Andersen, E. Rienks, M. Bianchi, M. Fanetti, E. Laegsaard, A. Baraldi, S. Lizzit, Z. Sljivancanin, F. Besenbacher, B. Hammer, T. G. Pedersen, P. Hofmann, L. Hornekaer, *Nat. Mater.* **2010**, *9*, 315.
[15] D. Haberer, D. V. Vyalikh, S. Taioli, B. Dora, M. Farjam, J. Fink, D. Marchenko, T. Pichler, K. Ziegler, S. Simonucci, M. S. Dresselhaus, M. Knupfer, B. Büchner, A. Grüneis, *Nano Lett.* **2010**, *10*, 3360.
[16] R. R. Nair, W. Ren, R. Jalil, I. Riaz, V. G. Kravets, L. Britnell, P. Blake, F. Schedin, A. S. Mayorov, S. Yuan, M. I. Katsnelson, H.-M. Cheng, W. Strupinski, L. G. Bulusheva, A. V. Okotrub, I. V. Grigorieva, A. N. Grigorenko, K. S. Novoselov, A. K. Geim *Small* **2010**, *6*, 2877.
[17] K.-J. Jeon, Z. Lee, E. Pollak, L. Moreschini, A. Bostwick, C.-M. Park, R. Mendelsberg, V. Radmilovic, R. Kostecki, T. J. Richardson, E. Rotenberg, *ACS Nano* **2011**, *5*, 1042.
[18] D. Usachov, O. Vilkov, A. Grüneis, D. Haberer, A. Fedorov, V. K. Adamchuk, A. B. Preobrajenski, P. Dudin, A. Barinov, M. Oehzelt, C. Laubschat, D. V. Vyalikh, *Nano Lett.* **2011**, *11*, 5401.

[19] L. Zhao, R. He, K. T. Rim, T. Schiros, K. S. Kim, H. Zhou, C. Gutiérrez, S. P. Chockalingam, C. J. Arguello, L. Pálová, D. Nordlund, M. S. Hybertsen, D. R. Reichman, T. F. Heinz, P. Kim, A. Pinczuk, G. W. Flynn, A. N. Pasupathy, *Science* **2011**, *333*, 999.
[20] E. Starodub, N. C. Bartelt, K. F. McCarty, *J. Phys. Chem. C* **2010**, *114*, 5134.
[21] N. A. Vinogradov, K. Schulte, M. L. Ng, A. Mikkelsen, E. Lundgren, N. Martensson, A. B. Preobrajenski, *J. Phys. Chem. C* **2011**, *115*, 9568.
[22] W. Zhang, A. Nefedov, M. Naboka, L. Cao, C. Wöll, *Phys. Chem. Chem. Phys.* **2012**, *116*, 10125.
[23] F. Simon, C. Kramberger, R. Pfeiffer, H. Kuzmany, V. Zolyomi, J. Kurti, P. M. Singer, H. Alloul, *Phys. Rev. Lett.* **2005**, *95*, 017401.
[24] A. Nagashima, N. Tejima, C. Oshima, *Phys. Rev. B* **1994**, *50*, 17487.
[25] A. Grüneis, K. Kummer, D. V. Vyalikh, *New J. Phys.* **2009**, *11*, 073050.
[26] T. Zecho, A. Güttler, X. Sha, B. Jackson, J. J. Küppers, *Chem. Phys.* **2002**, *117*, 8486.
[27] T. Zecho, A. Güttler, X. Sha, D. Lemoine, B. Jackson, J. Küppers, *Chem. Phys. Lett.* **2002**, *366*, 188.
[28] V. Barone, F. Lelj, C. Minichino, N. Russo, M. Toscano, *Surf. Sci.* **1987**, *185*, 189–190.
[29] N. Russo, M. Toscano, *J. Mol. Struct.: THEOCHEM* **1989**, *201*, 149.
[30] S. Casolo, O. M. Lovvik, R. Martinazzo, G. F. Tantardini, *J. Chem. Phys.* **2009**, *130*, 054704.
[31] C. P. Herrero, R. Ramirez, *Phys. Rev. B* **2009**, *79*, 115429.
[32] A. H. C. Neto, F. Guinea, N. M. R. Peres, K. S. Novoselov, A. K. Geim, *Rev. Mod. Phys.* **2009**, *81*, 109.
[33] A. Varykhalov, J. Sanchez-Barriga, A. M. Shikin, C. Biswas, E. Vescovo, A. Rybkin, D. Marchenko, O. Rader, *Phys. Rev. Lett.* **2008**, *101*, 157601.
[34] K. Jousten, P. Röhl, *Vacuum* **1995**, *46*, 9.
[35] L. Petaccia, P. Vilmercati, S. Gorovikov, M. Barnaba, A. Bianco, D. Cocco, C. Masciovecchio, A. Goldoni, *Nucl. Instrum. Meth. A* **2009**, *606*, 780.
[36] Y. Wang, H. J. Qian, K. Morokuma, S. Irle, *J. Phys. Chem. A* **2012**, *116*, 7154.